JOURNAL OF AIRCRAFT
Vol. 44, No. 5, September–October 2007

Application of CFD-Based Unsteady Forces for Efficient Aeroelastic Stability Analyses

Alexandre Noll Marques*
Instituto Tecnológico de Aeronáutica, 12228-900 São José dos Campos, Brazil
and
João Luiz F. Azevedo†
Instituto de Aeronáutica e Espaço, 12228-903 São José dos Campos, Brazil

DOI: 10.2514/1.27510

The present work is aimed at developing a methodology for aeroelastic analysis of lifting surfaces in the transonic regime using an unsteady computational fluid dynamics tool for the calculation of the aerodynamic operator. The applied computational fluid dynamics tool solves the flow problem modeled by the two-dimensional Euler equations using the finite volume method applied in an unstructured grid context. The proposed methodology is based on the determination of the aerodynamic operator with the transfer function technique, which is given, in the frequency domain, by the analysis of the system response to an exponentially shaped pulse in the time domain. The response in the frequency domain is obtained with the fast Fourier transform technique available in any mathematical manipulation tool. Numerical experiments are performed involving unsteady subsonic and transonic flows around a flat plate and a NACA 0012 airfoil and the results are presented as curves of aerodynamic generalized forces. The respective Fourier transforms are also determined and then compared with data available in the literature. Aeroelastic analyses are presented and discussed for the typical section case based on both geometries. Finally, a discussion is presented of theoretical questions concerning the understanding of a computational fluid dynamics solver as a discrete-time system and its relevant properties, and the correct aerodynamic input for the efficient computation of the frequency domain responses.

Nomenclature

a_h	=	dimensionless distance from midchord to elastic axis
b	=	airfoil semichord, $c/2$
c	=	airfoil chord
k	=	reduced frequency, $\omega b/U_\infty$
k_h	=	flexural stiffness constant
k_α	=	torsional stiffness constant
M_∞	=	undisturbed flow Mach number
m	=	airfoil mass
Q^*	=	dimensionless dynamic pressure, U^{*2}/μ
r_α	=	dimensionless airfoil radius of gyration about elastic axis
U_∞	=	undisturbed flow velocity
U^*	=	dimensionless flow velocity, $U_\infty/b\omega_\alpha$
x_α	=	dimensionless distance from elastic axis to mass center
α_0	=	initial angle of attack
μ	=	airfoil mass ratio, $m/\pi\rho b^2$
ω	=	angular frequency

I. Introduction

AEROELASTICITY can be defined as the science which studies the mutual interaction between aerodynamic, elastic, and inertial forces. The analysis of dynamic characteristics of either complex or simple structures is quite developed nowadays as far as numerical and experimental methods are concerned. Hence, it is correct to state that reliability in aeroelastic calculations is strongly dependent on the correct evaluation of the aerodynamic operator.

Traditionally, the methods developed for determining the aerodynamic operator for subsonic and supersonic regimes are based on linearized formulations which do not present the same satisfactory results in the transonic range. According to Tijdeman [1], this occurs due to the nonlinearity of transonic flows characterizing a significant alteration of the flow behavior, even when a profile is submitted to small perturbations. Ashley [2] reported the use of semi-empirical corrections to the linearized theory results as a means of improving flutter predictions. Nevertheless, Ashley himself believed that really satisfactory aeroelastic quantitative predictions of the transonic regime should be possible only when accurate, three-dimensional, unsteady computational fluid dynamics (CFD) codes were completely developed. Hence, the methodology here presented, which is based on the ideas of Rausch et al. [3] and Oliveira [4], intends to obtain the aerodynamic operator for two-dimensional lifting surfaces employing modern CFD techniques.

Computational fluid dynamics is a subject that has played an extremely important role in recent studies of aerodynamics. The possibility of numerically treating a broad range of phenomena which occur in flows over bodies of practically any geometry has numerous advantages over experimental determinations, such as greater flexibility together with time and financial resource savings. However, obtaining more reliable numerical results for a growing number of situations has been one of the major recent challenges in many science fields. Fletcher [5] and Hirsch [6] show that particularly in aerodynamics, the general phenomena are governed by the Navier–Stokes equations, which constitute a system of coupled nonlinear partial differential equations that has no general analytical solution. Hirsch comments, among other issues concerning CFD techniques, on how to simplify the mathematical models conveniently to ease the numerical treatment of each case. Space and time discretization schemes, as well as convergence acceleration techniques, boundary condition definition, and other numerical integration tools are available and largely used to solve

Presented as Paper 0250 at the 44th AIAA Aerospace Sciences Meeting and Exhibit, Reno, NV, 9–12 January 2006; received 26 August 2006; revision received 29 December 2006; accepted for publication 4 January 2007.

*Master of Science Student, Division of Aeronautical Engineering, Instituto Tecnológico de Aeronáutica, Centro Técnico Aeroespacial; ale_noll@yahoo.com. Student Member AIAA.

†Senior Research Engineer, Centro Técnico Aeroespacial. Currently Director for Space Transportation and Licensing, Brazilian Space Agency, 70610-200 Brasília, Brazil; azevedo@iae.cta.br. Associate Fellow AIAA.

such models. After selection of the theoretical model, it is necessary to define the physical domain where the flows take place, characterizing the boundary conditions. This flow solution approach demands the discrete representation of the physical domain to make the problems numerically coherent defining a computational mesh of points or regions where the calculations are performed. The mesh generation, as it is vastly documented in the literature, e.g., Fletcher [7], is extremely important and decisive in the accuracy and convergence of the solution. The mesh type is also an essential factor of the CFD tool behavior. Structured meshes have the advantage of being well behaved, the existence of an intrinsic correspondence between adjacent nodes and a very good control over grid refinement through stretching functions. However, this sort of mesh does not readily adapt to complicated geometries, requiring the adoption of more sophisticated multiblock mesh techniques. On the other hand, unstructured meshes are extremely flexible when it comes to geometric forms and they allow the use of interesting techniques such as solution adaptive refinement.

As stated in [8], together with the evolution of the work and projects performed by Instituto de Aeronáutica e Espaço (CTA/IAE), the demand for aerodynamic parameters has swelled, mainly those concerning the vehicles developed at this organization. Nevertheless, the application of CFD tools in these parameter analyses has always been limited by the need of adequate code development and the lack of computational resources compatible with the work to be performed. Therefore, a progressive approach has been adopted in the development of CFD tools at CTA/IAE and Instituto Tecnológico de Aeronáutica, as presented in [4,9–15].

The present work is based on using CFD to provide the aerodynamic operator for aeroelastic analysis in an efficient fashion. Here, a CFD tool is applied with unstructured two-dimensional meshes around lifting surfaces to obtain unsteady responses to harmonic, exponentially-shaped pulse, unit sample, and discrete step motions. The methodology here presented intends to obtain frequency domain responses from time domain solutions. Such responses supply the generalized aerodynamic forces necessary as input to the aeroelastic model. Therefore, with that information, it is possible to determine the aeroelastic stability margin with a single expensive CFD run for each structural mode. Moreover, the use of these four excitations is made to address theoretical questions concerning the correct input for the efficient calculation of the frequency domain responses. Furthermore, there is also interest in considering the compatibility of continuous and discrete-time signals, hence addressing the ideas presented in [4,16–18]. The correct assessment of such questions is of major importance in the area of reduced-order models for aeroelastic and aeroservoelastic applications.

II. Aerodynamic Theoretical Formulation

The CFD tool applied in this work is based on the two-dimensional Euler equations, which represent two-dimensional, compressible, rotational, inviscid, and nonlinear flows. Therefore, it is completely capable of capturing the shock waves present in transonic flows. Because of the use of unstructured meshes and the adoption of the finite volume approach, these equations are written in Cartesian form. Furthermore, as usual in CFD applications, flux vectors are employed and the equations are nondimensionalized. Hence, they can be written as

$$\frac{\partial}{\partial t}\iint_V \boldsymbol{Q}\,\mathrm{d}x\,\mathrm{d}y + \int_S (\boldsymbol{E}\,\mathrm{d}y + \boldsymbol{F}\,\mathrm{d}x) = 0 \tag{1}$$

In Eq. (1), V represents the control volume or, more precisely, its area in the two-dimensional case; S is its surface, or its two-dimensional side edges; and $\boldsymbol{Q}$ is the vector of conserved properties of the flow, given by

$$\boldsymbol{Q} = \{\,\rho \quad \rho u \quad \rho v \quad e\,\}^T \tag{2}$$

$\boldsymbol{E}$ and $\boldsymbol{F}$ are the inviscid flux vectors in the x and y directions, respectively, defined as

$$\boldsymbol{E} = \begin{Bmatrix} \rho U \\ \rho u U + p \\ \rho v U \\ (e+p)U + x_t p \end{Bmatrix}, \qquad \boldsymbol{F} = \begin{Bmatrix} \rho V \\ \rho u V \\ \rho v V + p \\ (e+p)V + y_t p \end{Bmatrix} \tag{3}$$

The nomenclature adopted here is the usual in CFD: ρ is the density, u and v are the Cartesian velocity components, and e is the total energy per unity volume. The pressure p is given by the perfect gas equation, written as

$$p = (\gamma - 1)\left[e - \frac{1}{2}\rho(u^2 + v^2)\right] \tag{4}$$

Once again, as usual, γ represents the ratio of specific heats. The contravariant velocity components U and V are determined by

$$U = u - x_t \quad \text{and} \quad V = v - y_t \tag{5}$$

where x_t and y_t are the Cartesian components of the mesh velocity in the unsteady case. For further details on the theoretical formulation, such as boundary and initial conditions, the interested reader should refer to [8].

III. Numerical Formulation

The algorithm presented here is based on a cell-centered, finite volume scheme in which the stored information is actually the average value of the conserved properties throughout the entire control volume. These mean values are defined as

$$\boldsymbol{Q}_i = \frac{1}{V_i}\iint_{V_i} \boldsymbol{Q}\,\mathrm{d}x\,\mathrm{d}y \tag{6}$$

Equation (1) can then be rewritten for each ith cell as

$$\frac{\partial}{\partial t}(V_i \boldsymbol{Q}_i) + \int_{S_i} (\boldsymbol{E}\,\mathrm{d}y - \boldsymbol{F}\,\mathrm{d}x) = 0 \tag{7}$$

The remaining integration in Eq. (7) represents the flux of the vector quantities $\boldsymbol{E}$ and $\boldsymbol{F}$ through each control volume boundary. This code was developed to be used with unstructured meshes composed of triangles. The flux, therefore, can be evaluated as the sum of the flux contributions of each edge, which is obtained approximately from the average of the neighboring conserved quantities, as proposed by Jameson and Mavriplis [19]. Hence, the convective operator C is defined and given by

$$\int_{S_i} (\boldsymbol{E}\,\mathrm{d}y - \boldsymbol{F}\,\mathrm{d}x) = C(\boldsymbol{Q}_i) = \sum_{k=1}^{3} [\boldsymbol{E}(\boldsymbol{Q}_{ik})(y_{k_2} - y_{k_1}) - \boldsymbol{F}(\boldsymbol{Q}_{ik})(x_{k_2} - x_{k_1})] \tag{8}$$

where

$$\boldsymbol{Q}_{ik} = \frac{1}{2}(\boldsymbol{Q}_i + \boldsymbol{Q}_k) \tag{9}$$

and the (x_{k_1}, y_{k_1}) and (x_{k_2}, y_{k_2}) coordinates are relative to the vertices which define the interface between the cells.

The Euler equations are a set of nondissipative hyperbolic conservation laws. Thus, as discussed by Pulliam [20], their numerical treatment requires an inherently dissipative discretization scheme or the introduction of artificial dissipation terms to avoid oscillations near shock waves and to damp high frequency uncoupled error modes. Oliveira [4] states that the flux evaluation method adopted in the present CFD tool is analogous to a centered difference scheme in finite difference formulation. In this case, Pulliam [20] shows that the addition of artificial dissipation terms is needed. Details on the adopted artificial dissipation scheme are given in [8].

The numerical solution is advanced in time using a second-order accurate, five-stage, explicit, hybrid scheme which evolved from the

consideration of Runge–Kutta time stepping schemes [21,22]. This scheme, already including the necessary terms to account for changes in cell area due to mesh motion or deformation [23], can be written as

$$
\begin{aligned}
\boldsymbol{Q}_i^{(0)} &= \boldsymbol{Q}_i^n \\
\boldsymbol{Q}_i^{(1)} &= \frac{V_i^n}{V_i^{n+1}}\boldsymbol{Q}_i^{(0)} - \Theta_1 \frac{\Delta t_i}{V_i^{n+1}}[C(\boldsymbol{Q}_i^{(0)}) - D(\boldsymbol{Q}_i^{(0)})] \\
\boldsymbol{Q}_i^{(2)} &= \frac{V_i^n}{V_i^{n+1}}\boldsymbol{Q}_i^{(0)} - \Theta_2 \frac{\Delta t_i}{V_i^{n+1}}[C(\boldsymbol{Q}_i^{(1)}) - D(\boldsymbol{Q}_i^{(1)})] \\
\boldsymbol{Q}_i^{(3)} &= \frac{V_i^n}{V_i^{n+1}}\boldsymbol{Q}_i^{(0)} - \Theta_3 \frac{\Delta t_i}{V_i^{n+1}}[C(\boldsymbol{Q}_i^{(2)}) - D(\boldsymbol{Q}_i^{(1)})] \\
\boldsymbol{Q}_i^{(4)} &= \frac{V_i^n}{V_i^{n+1}}\boldsymbol{Q}_i^{(0)} - \Theta_4 \frac{\Delta t_i}{V_i^{n+1}}[C(\boldsymbol{Q}_i^{(3)}) - D(\boldsymbol{Q}_i^{(1)})] \\
\boldsymbol{Q}_i^{(5)} &= \frac{V_i^n}{V_i^{n+1}}\boldsymbol{Q}_i^{(0)} - \Theta_5 \frac{\Delta t_i}{V_i^{n+1}}[C(\boldsymbol{Q}_i^{(4)}) - D(\boldsymbol{Q}_i^{(1)})] \\
\boldsymbol{Q}_i^{n+1} &= \boldsymbol{Q}_i^{(5)}
\end{aligned}
\tag{10}
$$

where the superscripts n and $n+1$ indicate that these are property values at the beginning and the end of the nth time step, respectively. Furthermore, Δt is the time step. The values used for the Θ coefficients, as suggested by Mavriplis [22], are

$$
\Theta_1 = \frac{1}{4}, \qquad \Theta_2 = \frac{1}{6}, \qquad \Theta_3 = \frac{3}{8}, \qquad \Theta_4 = \frac{1}{2}, \qquad \Theta_5 = 1 \tag{11}
$$

In Eq. (10) the convective operator, $C(\boldsymbol{Q})$, is evaluated at every stage of the integration process, but the artificial dissipation operator, $D(\boldsymbol{Q})$, is only evaluated at the two initial stages. This is done with the objective of saving computational time because the evaluation of the latter is rather expensive. As discussed by Jameson et al. [21], this type of procedure is known to provide adequate numerical damping characteristics while achieving the desired reduction in computational cost.

Steady-state solutions for the mean flight condition of interest must be obtained before the unsteady calculation can be started. Therefore, it is also important to guarantee an acceptable efficiency for the code in steady-state mode. In the present work, both local time stepping and implicit residual smoothing [19,24,25] are employed to accelerate convergence to steady state. More details on convergence acceleration techniques are found in [4,8].

IV. Mesh Generation and Movement

The meshes used in the present work were generated with the commercial grid generator ICEM CFD©, a very powerful tool capable of creating sophisticated meshes with very good refinement and grid quality control. Figure 1 shows samples of the meshes around a NACA 0012 profile and a flat plate which were employed to obtain the present results.

Unsteady calculations involve body motion and, therefore, the computational mesh should be somehow adjusted to take this motion into account. The approach adopted here is to keep the far-field boundary fixed and to move the interior grid points to accommodate the prescribed body motion. This is done following the ideas presented in [23], where it is assumed that each side of the triangle is modeled as a spring with constant stiffness inversely proportional to the length of the side. Hence, once points on the body surface have been moved and assuming that the far-field boundary is fixed, a set of static equilibrium equations can be solved for the position of the interior nodes [4]. Control volume areas for the new grid can then be computed. The mesh velocity components can also be evaluated considering the new and old point positions and the time step. For further details, the interested reader should refer to [8].

V. Aeroelastic Formulation

The test case considered in the present work is widely known and reported in the literature [4,26]. The dynamic system represented in the typical section is a rigid airfoil section with two degrees of freedom, plunging and pitching, subjected to aerodynamic, inertial, and elastic forces and moments. The governing equation of such dynamical system is given by

$$
[M]\{\ddot{\eta}(t)\} + [K]\{\eta(t)\} = \{Qa(t)\} \tag{12}
$$

where the generalized mass and stiffness matrices are, respectively, given by

$$
[M] = \begin{bmatrix} 1 & x_\alpha \\ x_\alpha & r_\alpha^2 \end{bmatrix}, \qquad [K] = \begin{bmatrix} \omega_h & 0 \\ 0 & r_\alpha^2 \omega_\alpha^2 \end{bmatrix} \tag{13}
$$

and the generalized coordinate and force vectors are, respectively,

$$
\{\eta(t)\} = \{\, \xi(t) \quad \alpha(t) \,\}^T, \qquad \{\boldsymbol{Q}a(t)\} = \left\{ \frac{\boldsymbol{Q}a_h(t)}{mb} \quad \frac{\boldsymbol{Q}a_\alpha(t)}{mb^2} \right\}^T \tag{14}
$$

where $\xi = h/b$ is the plunge mode coordinate and α is the pitch mode. In the previous equations, ω_h and ω_α are the free vibration circular frequencies of each mode, which are defined as

$$
\omega_h = \sqrt{\frac{k_h}{m}}, \qquad \omega_\alpha = \sqrt{\frac{k_\alpha}{I_\alpha}} \tag{15}
$$

Moreover, I_α denotes the section moment of inertia with respect to the elastic axis over which pitching takes place. Finally, the radius of

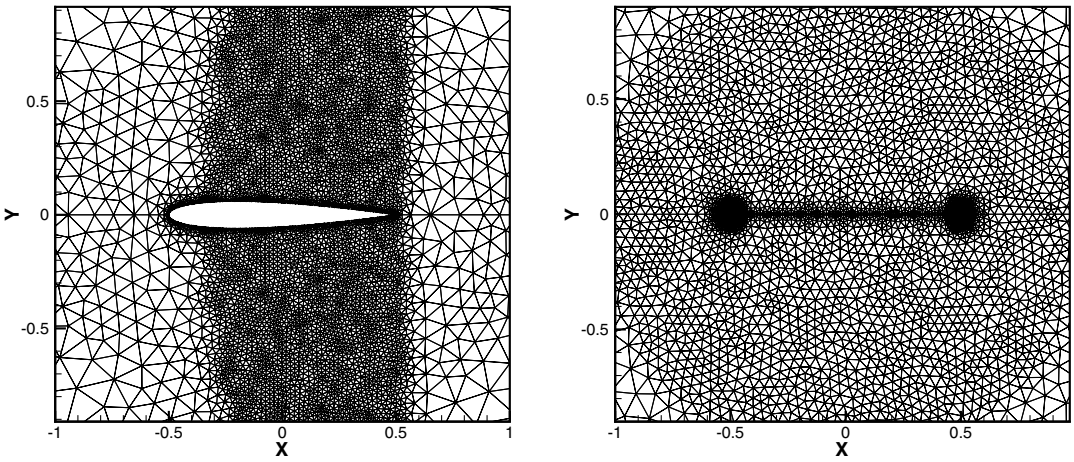

a) NACA0012 profile b) Flat plate

Fig. 1 Mesh around a) NACA 0012 profile with 292 wall points, and b) flat plate with 236 wall points.

gyration is given by

$$r_\alpha = \sqrt{\frac{I_\alpha}{mb^2}} \tag{16}$$

Considering the methodology proposed in Sec. VI, this system can be more easily studied in the Laplace domain. Applying the Laplace transform to Eq. (12), one can obtain

$$s^2[M]\{\eta(s)\} + [K]\{\eta(s)\} = \{\boldsymbol{Q}a(s)\} \tag{17}$$

Therefore, as mentioned previously, the main objective of the present study is to efficiently determine the generalized aerodynamic force vector $\{\boldsymbol{Q}a(s)\}$ in the Laplace domain for an arbitrary structural behavior. As will be shown, this is performed by evaluating this vector over the frequency range of interest and, by making use of the analytical continuation principle [27], extending such result to the entire s-plane. As presented by Oliveira [4], assuming linearity with regard to the modal motion, one can write

$$\{\boldsymbol{Q}a(s)\} = \frac{U_\infty^2}{\pi\mu b^2}[A(s)]\{\eta(s)\} \tag{18}$$

The aerodynamic influence coefficient matrix $[A(s)]$ is given by

$$[A(s)] = \begin{bmatrix} -Cl_h(s)/2 & -Cl_\alpha(s) \\ -Cm_h(s) & 2Cm_\alpha(s) \end{bmatrix} \tag{19}$$

where the α and h subscripts indicate the pitch and plunge mode contributions, respectively.

VI. Aeroelastic Analysis Methodology

The unsteady movements related to the aeroelastic phenomena, mainly flutter, can be represented by a series of harmonic motions. Therefore, the construction of the aerodynamic operator results from the evaluation of aerodynamic responses to harmonic excitations of various frequencies. However, instead of performing many expensive computational simulations for different frequencies, a large computational cost reduction can be obtained with the use of impulse or indicial excitations. As shown in [28], the impulse and indicial functions are capable of uniformly exciting the entire frequency domain simultaneously.

Therefore, the aerodynamic calculations for a determined flight condition are reduced to a single computational run for each structural mode. Moreover, the only hypotheses adopted are that the aerodynamic generalized forces are linear with regard to the motion amplitudes and that the total structural displacement can be obtained from the linear superposition of all individual modal displacements. However, this methodology captures the flow nonlinearities and dynamics according to the aerodynamic model applied, and the linear results are obtained by keeping the motion amplitude very low. Furthermore, as the Euler formulation is used in the present work, one cannot expect for nonlinearities related to viscous effects.

Nevertheless, the theoretical impulse and indicial motions are defined as singularities, a fact which has led researchers, at least until very recently, to believe that they were both numerically intractable [4,17]. Hence, other smoother excitation functions have been employed [16,29] to overcome such numerical problems. The motion used here is the one suggested in [17], which is defined as

$$f_p(\bar{t}) = \begin{cases} 4\left(\frac{\bar{t}}{\bar{t}_{\max}}\right)^2 \exp\left(2 - \frac{1}{1-\frac{\bar{t}}{\bar{t}_{\max}}}\right), & 0 \le \bar{t} < \bar{t}_{\max} \\ 0, & \bar{t} \ge \bar{t}_{\max} \end{cases} \tag{20}$$

where the bar indicates the dimensionless time and $\bar{t}_{\max}$ is the excitation duration. As can be seen in Fig. 2, the function defined in Eq. (20) guarantees a smooth motion.

However, there is recent work [18,30,31] which shows that a more suitable approach exists to understand computational aerodynamic responses. Such work points out the fact that once the aerodynamic model is represented through a numerical scheme, it becomes a discrete-time system rather than a continuous-time system. The consequences of such fact are explained in Sec. VII, but for now it is convenient to cite that there are discrete-time signals that present completely equivalent properties to impulse and indicial excitations and they are known as unit sample and discrete step [18,32], respectively. These are not at all singularities and are very well defined for numerical applications such as CFD. Thus, it is important to address the CFD response to such excitations and to evaluate the most convenient excitation, whether exponentially-shaped pulse, unit sample, or discrete step. This is one of the issues this work attempts to cover.

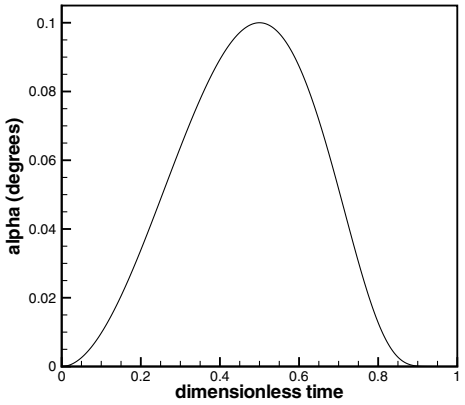

Fig. 2 Exponentially shaped pulse excitation in angle of attack.

The methodology consists, then, in obtaining a transfer function in the frequency domain applicable to any desirable input. This transfer function is the frequency domain response to the unit sample excitation. Therefore, this is accomplished using the following steps:

1) Obtain the steady aerodynamic solution for a given Mach number and angle of attack.

2) Perform unsteady aerodynamic response evaluations departing from the steady solution given in the preceding item. This stage leads to time responses in terms of aerodynamic coefficients as a result to excitations of each of the modes.

3) Obtain the discrete Fourier transform of the time responses applying a fast Fourier transform (FFT) algorithm. This is done in the present work employing the FFT capability available in the commercial program MATLAB®.

4) Approximate the obtained data with an interpolating polynomial.

5) Formulate the corresponding eigenvalue problem, valid for a determined range of dimensionless velocities, and, finally, perform flutter velocity prediction through a root locus analysis.

As shown by Oliveira [4], the corresponding frequency domain points resulting from the FFT procedure are given by

$$f[n] = \frac{1}{\Delta t}\frac{n}{N} = \frac{a_\infty}{\Delta \bar{t} c}\frac{n}{N}; \qquad n = 0, 1, 2, \ldots, N_{\max} \tag{21}$$

$$N\max = \begin{cases} N/2, & \text{if } N \text{ is even} \\ (N-1)/2, & \text{otherwise} \end{cases} \tag{22}$$

Equation (21), rewritten in terms of the reduced frequency based on the half-chord length, stands as

$$k = \frac{\omega b}{U_\infty} = \frac{2\pi f b}{U_\infty} \tag{23}$$

$$k[n] = \frac{\pi}{M_\infty \Delta \bar{t}}\frac{n}{N}; \qquad i = 0, 1, 2, \ldots, N_{\max} \tag{24}$$

As the exponentially shaped input is not a unit sample excitation, the real unit sample response is evaluated using a well-known property of the convolution theorem, as given in [32]:

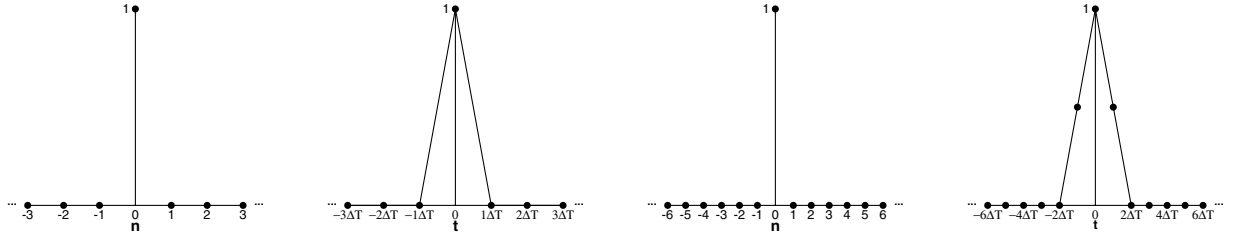

a) Unit sample sequence **b) Sampled triangular function** **c) Unit sample sequence with half the time step** **d) Sampled triangular function with half the time step**

Fig. 3 Differences between unit sample sequence and sampled function.

$$g[n] = f_p[n] * i[n] \rightarrow G[n] = F_p[n]I[n] \tag{25}$$

$$I[n] = \frac{G[n]}{F_p[n]} \tag{26}$$

where $i[n]$ represents the time response to a unit sample movement, $f_p[n]$ is the sequence that results from the sampling of the function in Eq. (20), and $g[n]$ is the response to the sampled exponentially shaped excitation. The sequences in capital letters are discrete Fourier transforms of the corresponding sequences in lower case letters. Therefore, after obtaining the FFT of the time response, it has to be divided by the FFT of the input sequence to obtain frequency domain responses. Although the input is not the exact unit sample excitation, it is capable of exciting the reduced frequencies of interest in aeroelastic studies.

The frequency domain responses obtained by these steps consist in a set of numerical values, which are not convenient for the solution of Eq. (17). Therefore, it is necessary to approximate these data using interpolating polynomials, as previously stated. The polynomial used in the present work is the one used by Karpel [33], Oliveira [4], and Abel [34]. It is originally proposed by Roger [35] and it is given, already in the Laplace domain, by

$$[A(s)] = [A_0] + [A_1]\left(\frac{b}{U_\infty}\right)s + [A_2]\left(\frac{b}{U_\infty}\right)^2 s^2 + \sum_{m=3}^{n} \frac{[A_m]s}{s + (U_\infty/b)\beta_{m-2}} \tag{27}$$

where β_m introduces the aerodynamic lags with respect to the structural modes, and they are arbitrarily selected from the range of reduced frequencies of interest. Moreover, $[A_m]$ are the approximating coefficient matrices given by a least squares optimization method, where $s = ikU_\infty/b$. Different ways of evaluating these matrices based on the same optimization principle are presented in [4,34]. Both ways result in the same interpolation polynomials when the same poles are used. There also are other suggestions of approximating polynomials, such as the approach given in [36], but they have not been tested by the present authors yet.

VII. CFD Solver as a Discrete-Time System

As aeronautical researchers are generally used to dealing with continuous-time problems, it has been very common in the literature to look at CFD solvers as mere approximations to continuous-time systems. Therefore, it is equally common to use continuous-time system properties and thinking when performing CFD simulations [4,16,17,29,37,38]. They are approximations, indeed, but discrete-time approximations. Hence, as shown by Silva [18], once the governing equations have been discretized, the resulting numerical scheme is actually a discrete-time system which has its own properties and peculiarities.

This mistake has led many authors [4,16,17,29] to justify the use of smooth pulse excitations because the theoretical continuous-time impulse and indicial excitations are not numerically feasible. Nevertheless, Silva [18] has suggested the use of equivalent discrete-time excitations: unit sample and discrete step [32]. Actually the term "step" is generally used rather than "discrete step," but this will be the terminology adopted throughout this paper to avoid confusion with the continuous-time indicial function. The unit sample sequence is given by

$$\delta[n] = \begin{cases} 0, & n \neq 0 \\ 1, & n = 0 \end{cases} \tag{28}$$

and the discrete step sequence is

$$u[n] = \begin{cases} 0, & n < 0 \\ 1, & n \geq 0 \end{cases} \tag{29}$$

or, equivalently,

$$u[n] = \sum_{i=-\infty}^{n} \delta[i] = \sum_{i=0}^{\infty} \delta[n-i] \tag{30}$$

Special attention must be paid not to confuse the unit sample with a sampled triangular continuous-time function. Figure 3 is an example of how different these can be. Figure 3a shows a standard unit sample sequence, and Fig. 3b a continuous triangular function with the corresponding samples. At first, both the sampled function and the unit sample sequence are identical. But now consider the same function sampled with a different time step, half of the original one. This is presented in Fig. 3d. However, the unit sample sequence input does not depend on the time step, what is demonstrated in Fig. 3c which is exactly the same as Fig. 3a, but with a different horizontal axis scale.

Such sequences formally hold properties very similar to the ones attributed to the impulse and step functions. Namely, if a linear time-invariant discrete system is submitted to a unit sample excitation, then the correspondent response will contain all the information about the system and the response to every other input is given by the following convolution sum [32]:

$$\text{out}[n] = \text{in}[n] * h[n] = \sum_{i=-\infty}^{\infty} \text{in}[i]h[n-i] = \sum_{i=-\infty}^{\infty} \text{in}[n-i]h[n] \tag{31}$$

where in$[n]$ is a generic input sequence, out$[n]$ is the respective response, and $h[n]$ is the system response to a unit sample input. It is very important to emphasize that, although the convolution sum given in Eq. (31) resembles the convolution integral[28], it is not an approximation to such integral, but a formally defined discrete operation. Moreover, the unit sample rigorously excites uniformly the complete frequency domain.

The discrete step response also characterizes a discrete system because one can reproduce the unit sample response from it. To demonstrate this fact, it is convenient to recall the convolution property

$$S[n] = u[n] * h[n] \tag{32}$$

Combining Eqs. (30) and (32), one obtains

$$S[n] = \sum_{j=-\infty}^{i} \sum_{i=-\infty}^{\infty} \delta[j]h[n-i] \tag{33}$$

Similarly,

$$S[n-1] = \sum_{j=-\infty}^{r} \sum_{r=-\infty}^{\infty} \delta[j]h[n-1-r] = \sum_{j=-\infty}^{i-1} \sum_{i=-\infty}^{\infty} \delta[j]h[n-i] \tag{34}$$

Finally, subtracting Eq. (34) from Eq. (32), one gets

$$S[n] - S[n-1] = \sum_{i=-\infty}^{\infty} \delta[i]h[n-i] = h[n] \tag{35}$$

Thus, theoretically, it would be more convenient, and even computationally cheaper (the transient solution should die out more rapidly), to acquire CFD results submitting the body to either unit-sample or discrete-step-type perturbations. This has been tried by some authors [18,30,31], but Raveh [31] has shown that some numerical complications may arise when simulating such cases. This occurs due to the large velocities induced by sharp motions, which may exceed the velocity the numerical time marching scheme can capture. Naturally, it all depends on the numerical formulation used in the CFD solver, input amplitude, and time step, but [18,30,31] demonstrate examples of a relatively successful application of this new approach. Additionally, Raveh [31] concludes that the discrete step excitation tends to be less sensitive to the simulation parameters than the unit sample.

All this reasoning does not invalidate the use of the exponentially shaped pulse, though it changes the way it is understood. This is because it should be put as a discrete input sequence derived from sampling the continuous function. However, it is obvious that, in the face of these new proposals, the authors are interested in evaluating their usage with the present CFD solver and also in comparing results and efficiency. Such discussions are presented in the results part of this paper.

Another question raised in [18,38] concerns the correct definition of the aerodynamic input function. For the CAP-TSD code used in [18,38], which is based on a transonic small disturbance formulation, it is proposed that such function should be given by the downwash, which, for the excitation of a given mode, is written as [18]

$$w(x, y, t) = \phi'(x, y)\psi(t) + \phi(x, y)\dot{\psi}(t) \tag{36}$$

where $\phi(x, y)$ is the modeshape, $\phi'(x, y)$ is the slope of the modeshape, $\psi(t)$ is the generalized coordinate, and $\dot{\psi}(t)$ is its time derivative. Therefore, the input excitation may actually be interpreted as a two-channel input, i.e., each term is a separate input channel. This means that each channel should be excited individually using a unit sample or discrete step input and, for the linear case, the final solution would come from the superposition of both answers. Naturally, for an Euler flow solver, as the one employed in the present work, the downwash function is not used for the boundary condition as in the CAP-TSD code. However, the boundary condition implementation in Euler flow solvers reflects the exact same physical principle of the downwash function, which is the fact that flow must be tangent to the wall boundary and, more important, it also presents a two-term dependency.

The two-channel input argument ruins all of the procedure proposed in the preceding section of the present paper, which is based on the single-input premise. This is because it is not possible to employ a smooth input function without exciting the derivative term. Actually, the procedure could eventually work when the input function used is smooth enough such that its derivative is small. In such cases, neglecting the influence of the second term does not lead to relevant errors. But this is not true when the slopes of the modeshapes are zero, as in the case of the plunge mode in the typical section model. In that case, Silva [18] argues that the mentioned procedure would be incorrect.

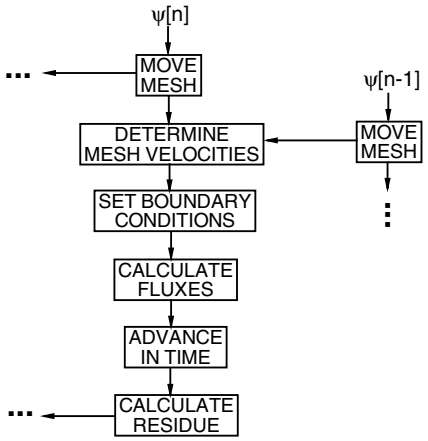

Fig. 4 Scheme of input role on establishment of boundary conditions.

Fortunately, the present authors have shown, in previous work [8], good results obtained applying the proposed methodology, even for the plunge mode. The explanation for such contradictory results lies on the fact that, for Euler or Navier–Stokes solvers, it is not necessary to separate the influence of the motion and its derivative into individual channels because they are not independent functions. This separation is obviously convenient to avoid dealing with the derivative of the discontinuous step and impulse functions. Actually, the latter is not a function in the common use of the word, but rather a type of function called "generalized function" [39], and the derivation of both becomes coherent only in certain integral applications. However, in the frequency domain, the relationship between the motion and its derivative can be easily seen through the Laplace transform of Eq. (36),

$$\begin{aligned} W(x, y, s) &= \phi'(x, y)\psi(s) + s\phi(x, y)\psi(s) \\ &= [\phi'(x, y) + s\phi(x, y)]\psi(s) \end{aligned} \tag{37}$$

Thus, the system depends only on the input ψ. Hence, although the system can be viewed to present multiple-channel inputs, the interpretation of ψ as a single-input is equivalent. Furthermore, as the new approach suggests the use of discrete-time sequences, there is no need to bother with such derivatives. As long as the time step is sufficiently small for a given frequency content, the approximation

$$\dot{\psi}[n] \approx \frac{\psi[n] - \psi[n-1]}{\Delta t} \tag{38}$$

holds. In other words, the velocity at any cell edge adjacent to a solid wall at iteration n depends only on the input value at iterations n and $n-1$. This approximation, however, is not explicitly implemented in the numerical algorithm. What is really done is schematically presented in Fig. 4. In Sec. VIII, some test cases are presented proving this reasoning to be correct.

There is also a discussion on the need to adjust generic excitations to properly excite the desired frequency range. However, for the exponentially shaped pulse, experience has shown it to be very straightforward and easy to use for the present case. Moreover, as mentioned before, although the unit step or discrete step theoretically should always work, there are numerical limitations with such inputs that also require a calibration procedure, if it is at all possible to overcome such limitations. Therefore, this need for adjustments of the exponentially shaped pulse is not really a disadvantage compared to other excitations.

VIII. Results and Discussion

Before attempting applications of the proposed methodology, some validation simulations are performed with the CFD tool. This has been done throughout the entire development of this code as can be seen in [4,8,15,40]. Once the CFD tool is tested and proved to be reliable, the next step is to proceed in obtaining the unsteady

Table 1 Flat plate test cases

Case	Mode	M_∞	α_0	Amplitude	Excitation	Width[a]	Time step[a]
1F	pitch	0.5	0.0	0.10 deg	exponentially shaped pulse	01	0.003
2F	plunge	0.5	0.0	0.01 c	exponentially shaped pulse	01	0.003

[a]In dimensionless time units

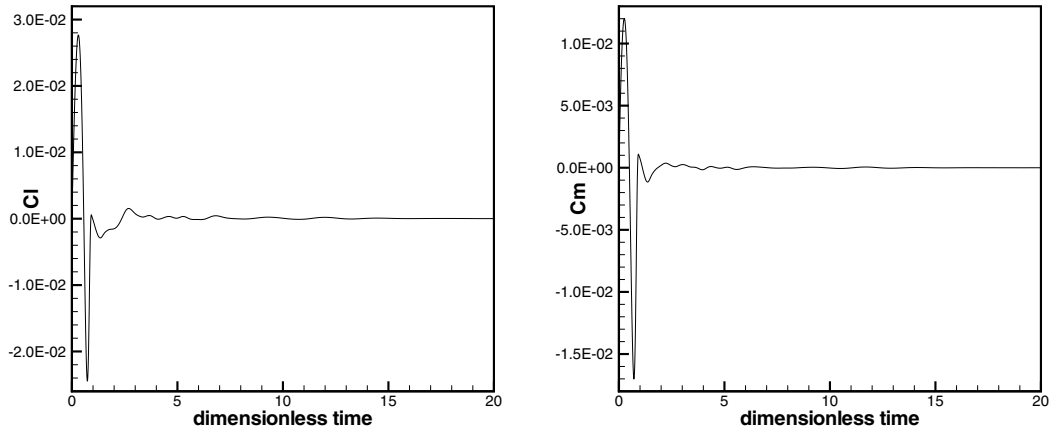

a) Cl time response b) Cm time response

Fig. 5 Time responses to case 1F (pitch mode exponentially shaped pulse excitation).

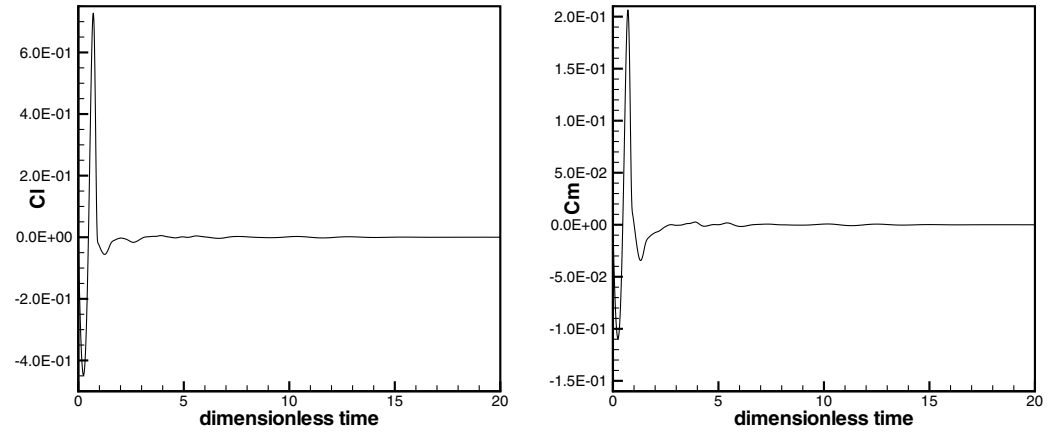

a) Cl time response b) Cm time response

Fig. 6 Time responses to case 2F (plunge mode exponentially shaped pulse excitation).

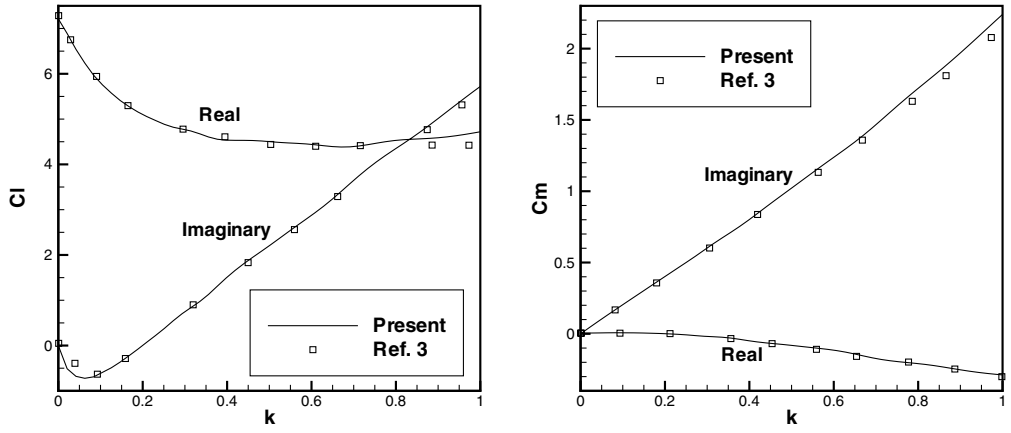

a) Cl frequency response b) Cm frequency response

Fig. 7 Frequency responses to case 1F.

responses of interest. The approach selected is to reproduce the numerical results presented by Rausch et al. [3].

A. Flat Plate

For the first set of simulations, an exponentially shaped excitation, as the one presented in Fig. 2, is used with a 1 dimensionless time unit width. Actually, although this is not demonstrated here, the authors have verified that, within a relatively large range, the pulse width has little influence in final frequency domain responses. Table 1 shows all the information on the two cases used when simulating the flat plate geometry. The pitch motion occurs about the quarter-chord point. The reader should note that, although this work is primarily aimed at the transonic regime, these purely subsonic cases provide good tests for the proposed methodology because there are reliable linearized solutions available.

The responses obtained are shown here in terms of the lift and moment coefficients, where the moment is measured about the

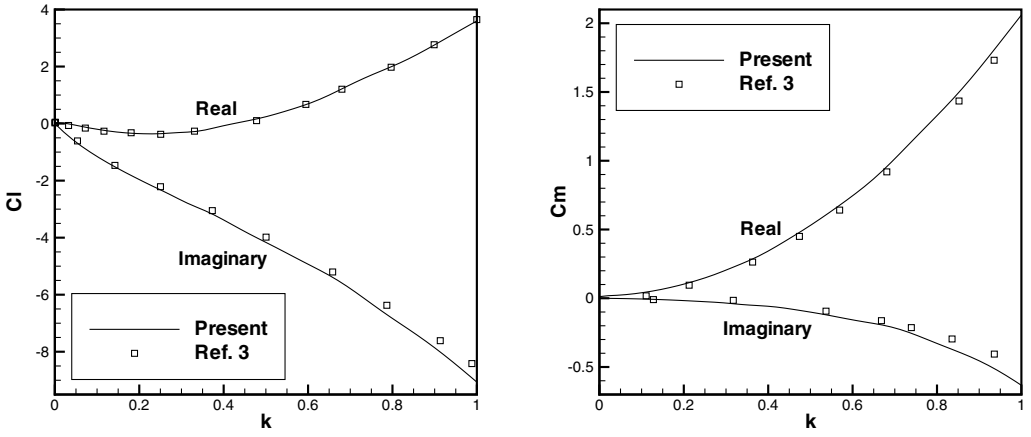

a) Cl frequency response b) Cm frequency response

Fig. 8 Frequency responses to case 2F.

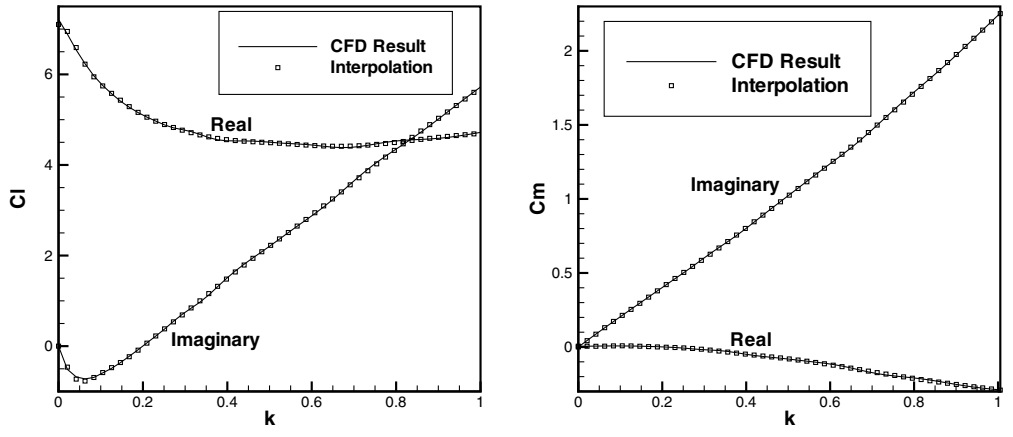

a) Approximate function for Cl b) Approximate function for Cm

Fig. 9 Approximating polynomials for the frequency responses to case 1F.

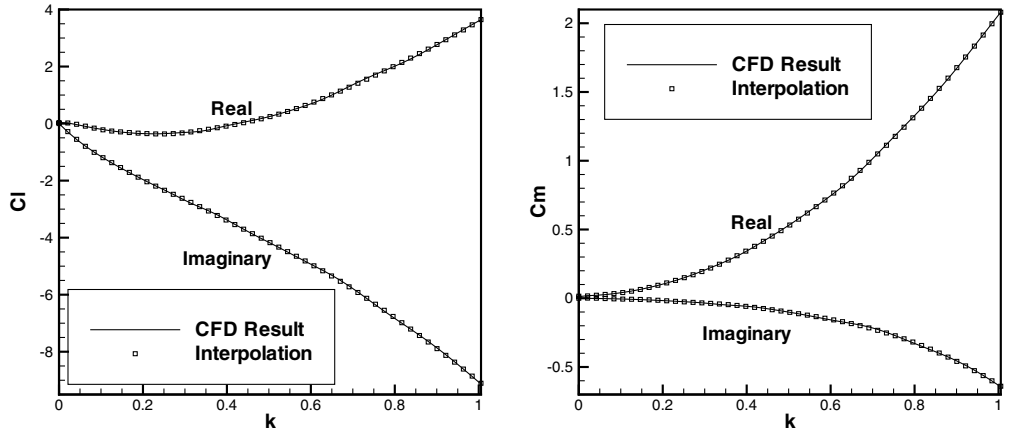

a) Approximate function for Cl b) Approximate function for Cm

Fig. 10 Approximating polynomials for the frequency responses to case 2F.

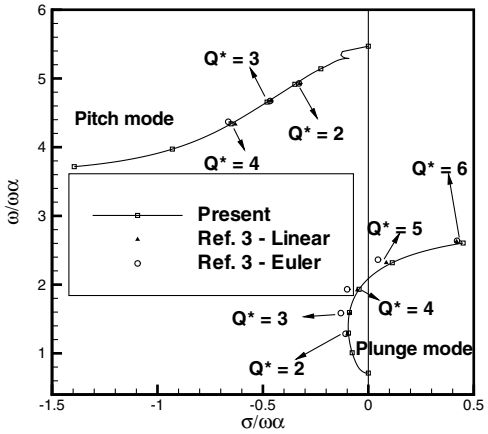

Fig. 11 Comparisons of dimensionless dynamic pressure root loci for the 1F and 2F cases.

quarter-chord point and it is positive in the nose-down direction. Figure 5 presents time responses for the pitch mode, whereas Fig. 6 presents time responses for the plunge one. It is relevant to note that no time response to this particular excitation is available in the literature. Hence, the results cannot be compared. Furthermore, these two cases are integrated up to 300 dimensionless time units, but only the first 20 dimensionless time units of such responses are shown to emphasize the most relevant part of the transient solution.

Table 2 Comparisons of flutter points for the 1F and 2F cases

Reference	Mode	U^*	Q^*	$\omega/\omega\alpha$
Present	plunge	16.4	4.5	2.08
Euler [3]	plunge	17.0	4.8	2.27
Linear [3]	plunge	16.6	4.6	2.10

The corresponding frequency domain responses, together with the numerical results given by Rausch et al. [3], also obtained with the Euler formulation, are shown in Figs. 7 and 8. These results show a very good agreement between calculations performed by the present authors and the literature data. Comparisons between results obtained with the Euler equations and the linear theory are presented in [3], and the agreement is fairly good for this case.

These results are interpolated with the use of 10 poles within the 0.001–0.99 reduced frequency range. The resulting polynomials are plotted in Figs. 9 and 10. It can be seen that the corresponding CFD results are perfectly represented by the polynomial approximations in the reduced frequency range of interest.

When these polynomials are substituted in Eq. (17), the aeroelastic problem is reduced to an eigenvalue problem as demonstrated in [4]. This problem depends on the dimensionless velocity parameter. The solution of such eigenvalue problem yields a root locus which is given in Fig. 11 as a function of the dimensionless dynamic pressure parameter. The eigenvalues are nondimensionalized with ω_α, and their real and imaginary parts are denoted by σ and ω, respectively. Indicated computational points in the root loci are separated by $\Delta Q^* = 1$. The flutter points occur when the real part of one of the eigenvalues becomes zero, characterizing undamped oscillations. The flutter point obtained in this case is compared with those of [3] in Table 2. The three given root loci and respective flutter points agree very well, as one could expect from the similarity of the frequency domain results. This example shows the coherence of the proposed methodology and of the CFD solver results.

B. NACA 0012 Airfoil

The authors perform a similar analysis for a NACA 0012 airfoil in the transonic regime. Comparison results for this case are also found in [3]. In this case, more than one excitation sequence is used. Table 3 shows the several cases simulated for the NACA 0012 configuration. Again, as in the flat plate cases, the pitch motion occurs about the quarter-chord point.

The time responses for these cases are presented in Figs. 12–17. The total integration time at all cases is 300 dimensionless time units,

Table 3 NACA 0012 test cases

Case	Mode	M_∞	α_0	Amplitude	Excitation	Width[a]	Time step[a]
1N	pitch	0.8	0.0	0.10 deg	EP	01	0.003
2N	plunge	0.8	0.0	0.001 c	EP	01	0.003
3N	pitch	0.8	0.0	0.0001 deg	US	——	0.003
4N	plunge	0.8	0.0	0.000001 c	US	——	0.003
5N	pitch	0.8	0.0	0.01 deg	DS	——	0.003
6N	plunge	0.8	0.0	0.0001 c	DS	——	0.003

[a]In dimensionless time units

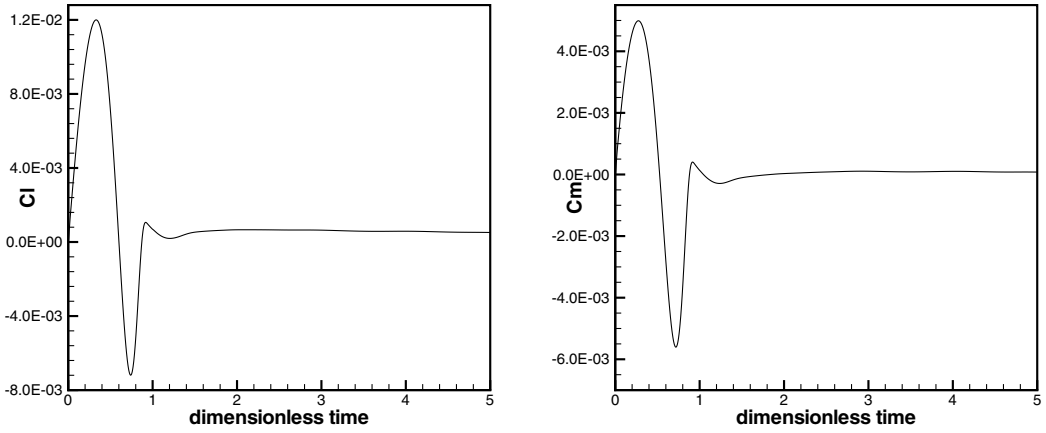

a) Cl response **b) Cm response**

Fig. 12 Time responses to case 1N (pitch mode exponentially shaped pulse excitation).

but only the most relevant parts of the solutions are presented. Furthermore, in case 5N, the solution converges to an asymptotic value different from the initial value. This occurs because the airfoil does not return to its initial configuration.

The frequency domain responses are shown in Figs. 18 and 19. A series of harmonic solutions for different reduced frequencies is also included to assess the correctness of these responses, at least within the CFD solution context. These harmonic (H) solutions are obtained imposing three cycles of harmonic motion to the body for each reduced frequency. However, only the third cycle is considered in the solution, because the first two cycles correspond to the transient part of the response. Moreover, one can easily see that the exponentially shaped (EP) excitation offers the best results. Although, in this case, the results obtained in the present study with the exponentially shaped pulse do not perfectly match the ones found in the literature [3], they are satisfactorily close. Furthermore, the agreement

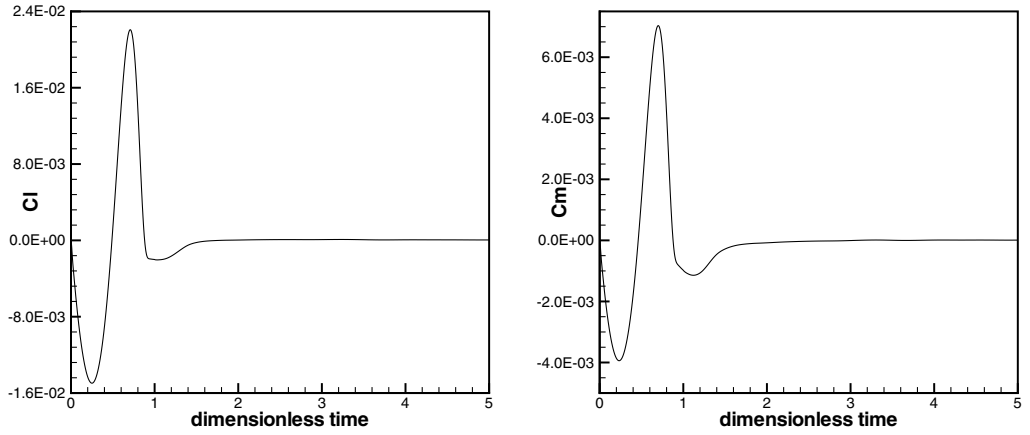

a) Cl response b) Cm response

Fig. 13 Time responses to case 2N (plunge mode exponentially shaped pulse excitation).

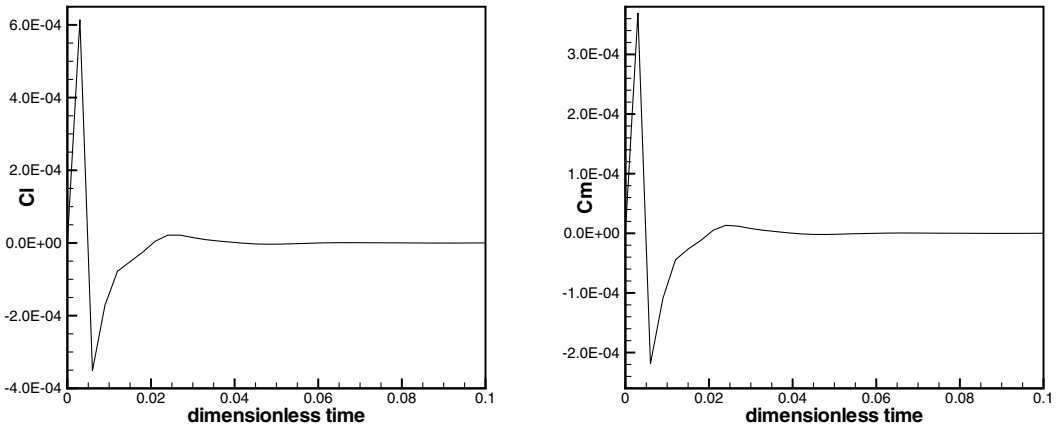

a) Cl response b) Cm response

Fig. 14 Time responses to case 3N (pitch mode unit sample excitation).

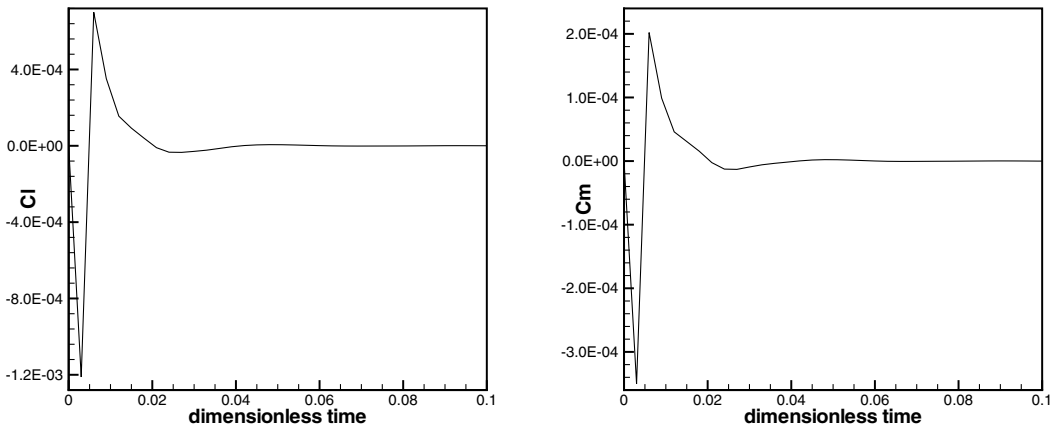

a) Cl response b) Cm response

Fig. 15 Time responses to case 4N (plunge mode unit sample excitation).

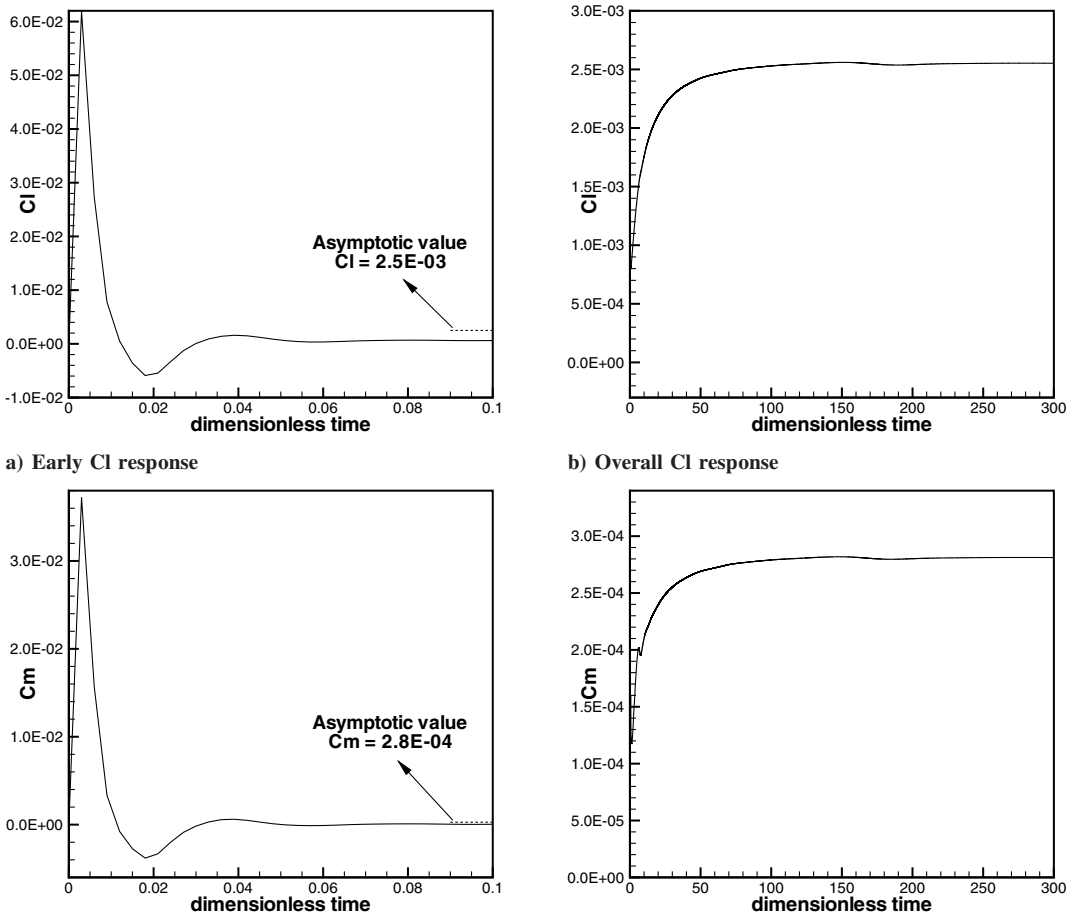

a) Early Cl response

b) Overall Cl response

c) Early Cm response

d) Overall Cm response

Fig. 16 Time responses to case 5N (pitch mode discrete step excitation).

between the exponentially shaped pulse responses and the harmonic ones, especially in the plunge mode, is a proof that the use of a single-channel input approach is correct in the context of an Euler solver.

When it comes to the discrete step (DS) and unit sample (US) responses, it is clear, especially for the plunge mode, that they do not agree with solutions given by other methods. However, the overall behavior is quite similar, which the authors believe to indicate that good solutions can be achieved. The subject still requires further investigation, but this is beyond the scope of the present paper.

Because only the responses to the exponentially shaped pulse come close to the expected values, the authors constructed interpolation polynomials only for cases 1N and 2N. The corresponding curves are shown in Figs. 20 and 21. In the present study, 15 poles are used in the 0.001–0.40 reduced frequency range. Once again, the polynomial interpolation process has shown to provide excellent results. Additionally, one may notice that although the reduced frequency range, where the poles are allocated, does not cover the entire range of approximated points, the resulting polynomial still holds as a close approximation. This occurs because all points are used in the least squares optimization. Therefore, one may concentrate the poles in the most convenient regions without compromising the overall results, just as demonstrated in this case.

Finally, with these results, it is possible to solve an aeroelastic problem submitted to a transonic flow. The eigenvalue problem is

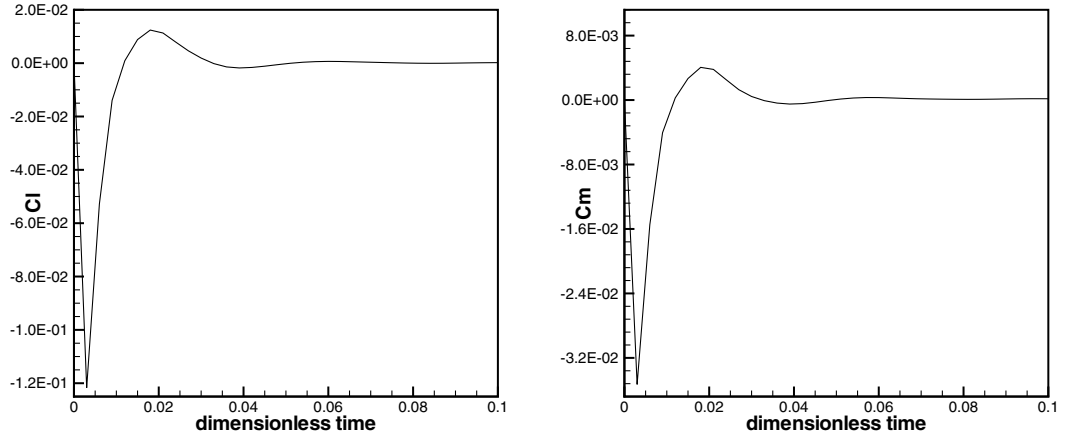

a) Cl response

b) Cm response

Fig. 17 Time responses to case 6N (plunge mode discrete step excitation).

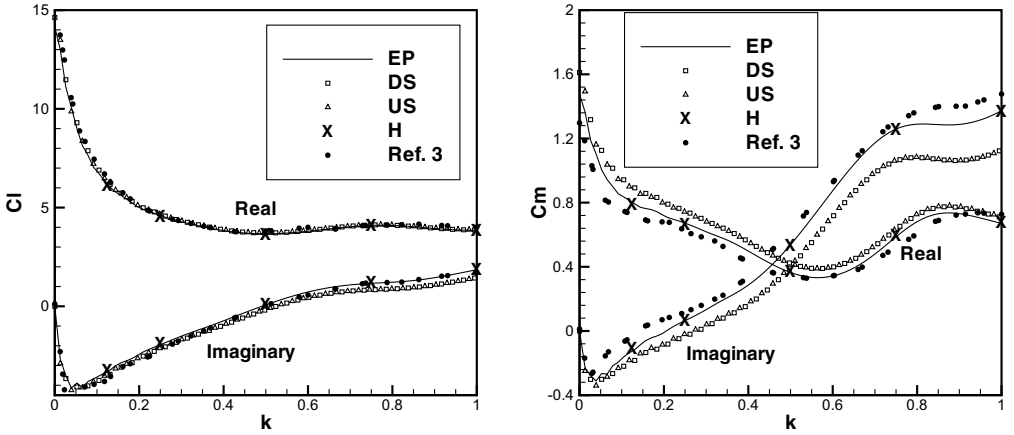

a) Cl response b) Cm response

Fig. 18 Frequency responses to cases 1N, 3N, and 5N (pitch mode excitation).

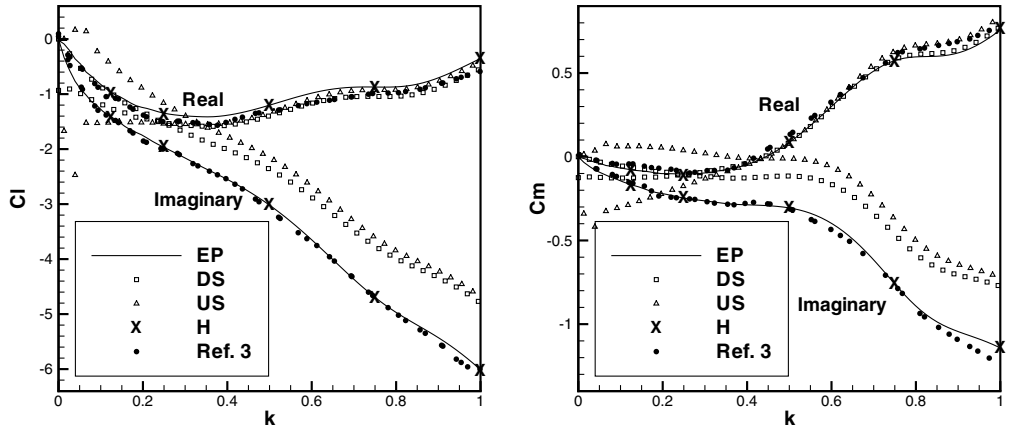

a) Cl response b) Cm response

Fig. 19 Frequency responses to cases 2N, 4N and 6N (plunge mode excitation).

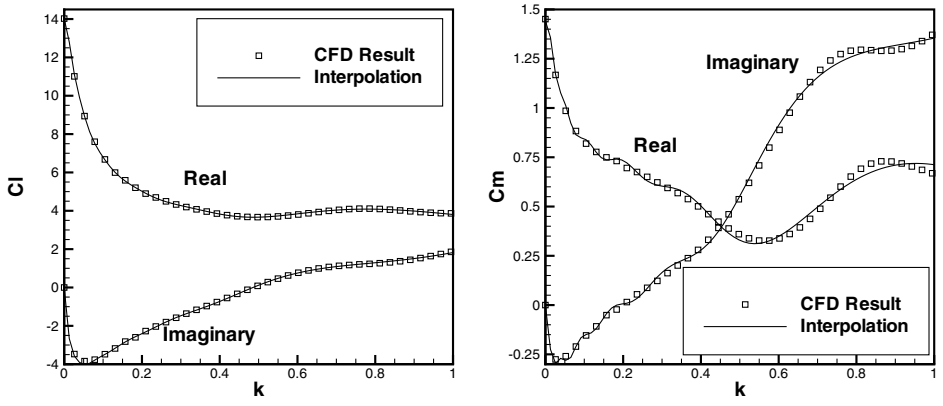

a) Approximate function for Cl b) Approximate function for Cm

Fig. 20 Approximating polynomials for frequency responses to case 1N (pitch mode excitation).

identical to the subsonic case [4]. The only difference lies in the aerodynamic coefficient matrix. The resulting root locus is presented in Fig. 22 with Q^* as parameter. Indicated computational points are separated by $\Delta Q^* = 0.1$. Data found in the literature [3] are also included. Once again, the agreement between the present results and those given in [3] is very good, at least for the plunge mode. A larger difference is seen in the pitch mode. However, it could be expected due to the differences presented in Fig. 18, especially in the moment coefficient, i.e., the pitch mode generalized force due to a pitch excitation. Furthermore, the flutter points are indicated in Table 4. Such values reinforce the solution agreement. It is important to notice the difference between flutter points indicated with the linear and Euler formulations. This is a typical example of how the linear theory may predict flutter speeds which are larger than the actual values for the flutter boundary, which is an unsafe result from the point of view of an engineer trying to perform the flutter clearance for a given configuration. Such decrease in the flutter speeds in the transonic regime characterizes the well-known "transonic dip" phenomenon.

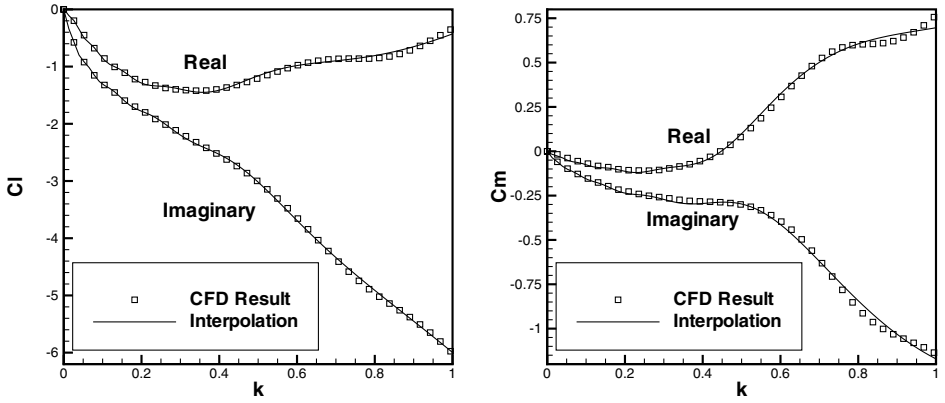

a) Approximate function for Cl b) Approximate function for Cm

Fig. 21 Approximating polynomials for the frequency responses to case 2N (plunge mode excitation).

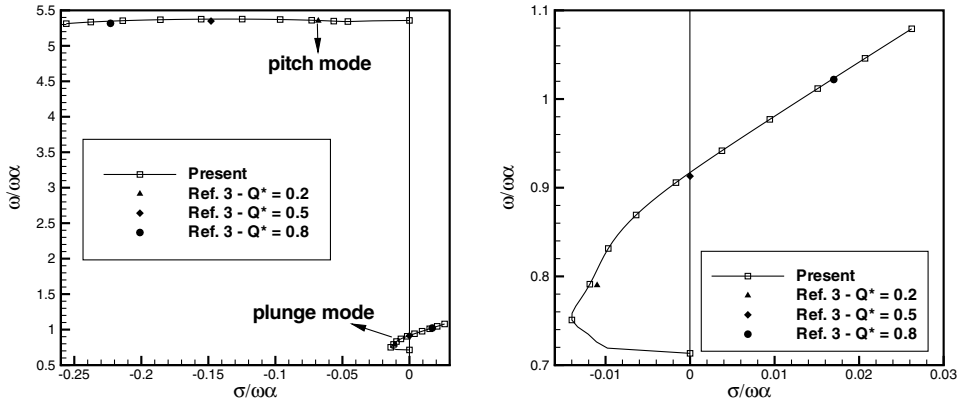

a) Root loci b) Plunge mode root loci

Fig. 22 Flutter root locus for a NACA 0012 typical section ($M_\infty = 0.8, \alpha_0 = 0$). On the right, a detailed view of the plunge mode root locus.

The ability to correctly predict the flutter condition within the transonic dip range of Mach numbers is the major motivation for the development of the present methodology.

IX. Conclusions

The paper has shown successful aeroelastic analysis results obtained using the proposed indicial methodology. All intermediary steps are also presented and discussed in detail. The results are a demonstration of the appropriateness of the proposed formulation and of the correct implementation of the entire methodology, providing the required capabilities to efficiently study aeroelastic stability problems using modern CFD tools. This is especially important for transonic cases, where the linear theory may overpredict the flutter velocity. Therefore, this work represents a fundamental evolution in the capability of performing numerical aeroelastic studies at CTA/IAE.

Moreover, the authors expect to have made contributions toward the solution of some of the current theoretical questions concerning this sort of approach in CFD-based analyses. The authors demonstrated, for instance, that a correct interpretation of the aerodynamic input function eliminates the need for a two-channel input formulation. Additionally, it is attempted to obtain results for appropriate discrete-time excitations. However, the determination of responses to the unit sample and discrete step inputs has yielded numerical difficulties that have not been completely solved yet. Therefore, it is still too early to draw conclusions about its use with the present CFD solver. Furthermore, it is important to emphasize that the closure of such questions is very relevant in many areas, particularly in the development of reduced-order models for aeroservoelastic control laws. Hence, the present paper is part of a work that aims at the improvement of the construction of aerodynamic reduced-order models for aeroelastic purposes.

Table 4 Comparison of flutter points for a NACA 0012 typical section ($M_\infty = 0.8, \alpha_0 = 0$)

Reference	Mode	U^*	Q^*	$\omega/\omega\alpha$
Present	plunge	5.64	0.53	0.92
CFL3D, Euler [3]	plunge	5.37	0.48	not informed
Linear [3]	plunge	10.65	1.89	not informed

Acknowledgments

The authors gratefully acknowledge the partial support for this research provided by Conselho Nacional de Desenvolvimento Científico e Tecnológico under the Integrated Project Research Grant No. 501200/2003-7. This work is also supported by Fundação de Amparo à Pesquisa do Estado de São Paulo through a Master of Science Scholarship for the first author according to Fundação de Amparo à Pesquisa do Estado de São Paulo Process No. 04/11200-1. Finally, the authors thank Carlos F. C. Simões for valuable discussions which were extremely important for the achievement of the present successful results.

References

[1] Tijdeman, H., "Investigation of the Transonic Flow Around Oscillating Airfoils," National Aerospace Lab., NLR-TR-77090U, The Netherlands, 1977.

[2] Ashley, H., "Role of Shocks in the "Sub-Transonic" Flutter Phenomenon," *Journal of Aircraft*, Vol. 17, No. 3, March 1980, pp. 187–197.

[3] Rausch, R. D., Batina, J. T., and Yang, H. T. Y., "Euler Flutter Analysis of Airfoil Using Unstructured Dynamic Meshes," *Journal of Aircraft*, Vol. 27, No. 5, May 1990, pp. 436–443.
[4] Oliveira, L. C., "State-Space Aeroelastic Analysis Methodology Using Computational Aerodynamics Techniques," M.S. Thesis, Instituto Tecnológico de Aeronáutica, São José dos Campos, São Paulo, Brazil, Aug. 1993 (in Portuguese).
[5] Fletcher, C. A. J., *Computational Techniques for Fluid Dinamics: Fundamental and General Techniques*, Vol. 1, Springer–Verlag, Heidelberg, Germany, 1988.
[6] Hirsch, C., *Numerical Computation of Internal and External Flows: Fundamentals of Numerical Discretization*, Vol. 1, Wiley, NY, 1989.
[7] Fletcher, C. A. J., *Computational Techniques for Fluid Dinamics: Specific Techniques for Different Flow Categories*, Vol. 2, Springer–Verlag, Heidelberg, Germany, 1988.
[8] Marques, A. N., "Simulation of Unsteady Aerospace Flows Using Unstructured Meshes," Graduation Project, Instituto Tecnológico de Aeronáutica, São José dos Campos, São Paulo, Brazil, Dec. 2004 (in Portuguese).
[9] Azevedo, J. L. F., "Euler Solutions of Transonic Nozzle Flows," *Proceedings of the 3rd National Meeting on Thermal Sciences: III ENCIT*, ABCM, Itapema, SC, Brazil, Dec. 1990, pp. 243–248.
[10] Azevedo, J. L. F., Fico, N. G. C. R., Jr., and Ortega, M. A., "Two-Dimensional and Axisymmetric Nozzle Flow Computation Using the Euler Equations," *Journal of the Brazilian Society of Mechanical Sciences and Engineering*, Vol. 17, No. 2, April–June 1995, pp. 147–170.
[11] Fico, N. G. C. R., Jr., and Azevedo, J. L. F., "Numerical Investigation of Supersonic Flow in a Slotted Wind Tunnel," *Proceedings of the 15th Iberian Latin-American Congress on Computational Methods for Engineering: XV CILAMCE*, Associação para Métodos Computacionais em Engenharia, Belo Horizonte, MG, Brazil, Dec. 1994, pp. 314–322.
[12] Azevedo, J. L. F., Strauss, D., and Ferrari, M. A. S., "Viscous Multiblock Simulations of Axisymmetric Launch Vehicle Flows," *Journal of Spacecraft and Rockets*, Vol. 36, No. 4, July–Aug. 1999, pp. 489–498.
[13] Bigarelli, E. D. V., Mello, O. A. F., and Azevedo, J. L. F., "Three-Dimensional Flow Simulations for Typical Launch Vehicles at Angle of Attack," *Proceedings of the 15th Brazilian Congress on Mechanical Engineering: COBEM 1999* [CD-ROM], ABCM, Águas de Lindóia, São Paulo, Brazil, Nov. 1999.
[14] Bigarelli, E. D. V., and Azevedo, J. L. F., "Turbulence Models for 3-D Aerospace Applications," *Proceedings of the 9th Brazilian Congress of Thermal Engineering and Sciences*, ABCM [CD-ROM], Caxambu, MG, Brazil, Paper CIT02-0341, Oct. 2002.
[15] Simões, C. F. C., and Azevedo, J. L. F., "Influence of Numerical Parameters on Unsteady Airfoil Inviscid Flow Simulations Using Unstructured Dynamic Meshes," *Proceedings of the 15th Brazilian Congress of Mechanical Engineering: COBEM 1999* [CD-ROM], ABCM, Águas de Lindóia, São Paulo, Brazil, Nov. 1999.
[16] Mohr, R. W., Batina, J. T., and Yang, H. T. Y., "Mach Number Effects on Transonic Aeroelastic Forces and Flutter Characteristics," *Journal of Aircraft*, Vol. 26, No. 11, Nov. 1989, pp. 1038–1046.
[17] Bakhle, M. A., Mahjan, A. J., Keith, T. G., and Stefko, G. L., "Cascade Flutter Analysis with Transient Response Aerodynamics," *Computers and Structures*, Vol. 41, No. 5, 1991, pp. 1073–1085.
[18] Silva, W. A., "Identification of Linear and Nonlinear Aerodynamic Impulse Responses Using Digital Filter Techniques," NASA, TM 112872, NASA Langley Research Center, Hampton, VA, Aug. 1997.
[19] Jameson, A., and Mavriplis, D., "Finite Volume Solution of the Two-Dimensional Euler Equations on a Regular Triangular Mesh," *AIAA Journal*, Vol. 24, No. 4, April. 1986, pp. 611–618.
[20] Pulliam, T. H., "Artificial Dissipation Models for the Euler Equations," *AIAA Journal*, Vol. 24, No. 12, Dec. 1986, pp. 1931–1940.
[21] Jameson, A., Schmidt, W., and Turkel, E., "Numerical Solution of the Euler Equations by Finite Volume Methods Using Runge–Kutta Time-Stepping Schemes," *14th AIAA Fluid and Plasma Dynamics Conference, Palo Alto, CA*, AIAA Paper 81-1259, June 1981.
[22] Mavriplis, D. J., "Accurate Multigrid Solution of the Euler Equations on Unstructured and Adaptive Meshes," *AIAA Journal*, Vol. 28, No. 2, Feb. 1990, pp. 213–221.
[23] Batina, J. T., "Unsteady Euler Airfoil Solutions Using Unstructured Dynamic Meshes," *27th AIAA Aerospace Sciences Meeting, Reno, NV*, AIAA Paper 89-0115, Jan. 1989.
[24] Jameson, A., and Baker, T. J., "Solution of the Euler Equation for Complex Configurations," AIAA Paper 83-1929, July 1983.
[25] Jameson, A., and Baker, T. J., "Improvements to the Aircraft Euler Method," *25th AIAA Aerospace Sciences Meeting, Reno, NV*, AIAA Paper 87-0452, Jan. 1987.
[26] Bisplinghoff, H. L., Ashley, H. L., and Halfman, R. L., *Aeroelasticity*, Addison–Wesley, Cambridge, MA, 1955.
[27] Churchill, R. V., *Complex Variables and Applications*, 3rd ed., McGraw–Hill, New York, 1974.
[28] Brigham, E. O., *Fast Fourier Transform and its Applications*, Prentice–Hall, Englewood Cliffs, NJ, 1988.
[29] Davies, D., and Salmond, D. J., "Indicial Approach to Harmonic Perturbations in Transonic Flow," *AIAA Journal*, Vol. 18, No. 8, Aug. 1980, pp. 1012–1014.
[30] Silva, W. A., and Raveh, D. E., "Development of Unsteady Aerodynamic State-Space Models from CFD-Based Pulse Responses," *42nd AIAA/ASME/ASCE/AHS/ASC Structures, Structural Dynamics, and Materials Conference*, AIAA Paper 2001-1213, April 2001.
[31] Raveh, D. E., "Reduced-Order Models for Nonlinear Unsteady Aerodynamics," *AIAA Journal*, Vol. 39, No. 8, Aug. 2001, pp. 1417–1429.
[32] Oppenheim, A. V., and Schafer, R. W., *Discrete-Time Signal Processing*, Prentice–Hall, Englewood Cliffs, NJ, 1989.
[33] Karpel, M., "Time-Domain Aeroservoelastic Modeling Using Weighted Unsteady Aerodynamic Forces," *Journal of Guidance, Control, and Dynamics*, Vol. 13, No. 1, Jan.–Feb. 1990, pp. 30–37.
[34] Abel, I., "Analytical Technique for Predicting the Characteristics of a Flexible Wing Equipped with an Active Flutter-Suppression System and Comparison with Wind-Tunnel Data," NASA, TP 1367, Hampton, VA, Feb. 1979.
[35] Roger, K. L., "Airplane Math Modeling Methods for Active Control Design," AGARD CP-228, Aug. 1977.
[36] Eversman, W., and Tewari, A., "Consistent Rational-Function Approximation for Unsteady Aerodynamics," *Journal of Aircraft*, Vol. 28, No. 9, Sept. 1991, pp. 545–552.
[37] Silva, W. A., "Application of Nonlinear Systems Theory to Transonic Unsteady Aerodynamic Responses," *Journal of Aircraft*, Vol. 30, No. 5, Sept.–Oct. 1993, pp. 660–668.
[38] Silva, W. A., "Extension of a Nonlinear Systems Theory to General-Frequency Unsteady Transonic Aerodynamic Responses," *34th AIAA/ASME/ASCE/AHS/ASC Structures, Structural Dynamics, and Materials Conference, La Jolla, CA*, AIAA Paper 93-1590, Apr. 1993.
[39] Davies, B., *Applied Mathematical Sciences: Integral Transforms and Their Applications*, Vol. 25, Springer–Verlag, New York, 1978.
[40] Azevedo, J. L. F., "Development of Unstructured Grid Finite Volume Solvers for High Speed Flows," Instituto de Aeronáutica e Espaço, São José dos Campos, Rept. NT-075-ASE-N/92, São Paulo, Brazil, Dec. 1992.